Hydrophilic modification of neural microelectrode arrays based on multi-walled carbon nanotubes

2010 Nanotechnology 21 485501

(http://iopscience.iop.org/0957-4484/21/48/485501)

Nanotechnology **21** (2010) 485501 (10pp) doi:10.1088/0957-4484/21/48/485501

Hydrophilic modification of neural microelectrode arrays based on multi-walled carbon nanotubes

Chang-Hsiao Chen[1], Huan-Chieh Su[2], Shih-Chang Chuang[1], Shiang-Jie Yen[2], Yung-Chan Chen[3], Yu-Tao Lee[1], Hsin Chen[3], Tri-Rung Yew[2], Yen-Chung Chang[1,4,5], Shih-Rung Yeh[4,5] and Da-Jeng Yao[1,6,7]

[1] Institute of NanoEngineering and MicroSystems, National Tsing Hua University, Hsinchu 30013, Taiwan
[2] Department of Materials Science and Engineering, National Tsing Hua University, Hsinchu 30013, Taiwan
[3] Department of Electrical Engineering, National Tsing Hua University, Hsinchu 30013, Taiwan
[4] Institute of Molecular Medicine, National Tsing Hua University, Hsinchu 30013, Taiwan
[5] Department of Life Sciences, National Tsing Hua University, Hsinchu 30013, Taiwan
[6] Department of Power Mechanical Engineering, National Tsing Hua University, Hsinchu 30013, Taiwan

E-mail: djyao@mx.nthu.edu.tw

Received 24 June 2010, in final form 27 September 2010
Published 4 November 2010
Online at stacks.iop.org/Nano/21/485501

Abstract

To decrease the impedance of microelectrode arrays, for neuroscience applications we have fabricated and tested MEA based on multi-walled carbon nanotubes. With decreasing physical size of a microelectrode, its impedance increases and charge-transfer capability decreases. To decrease the impedance, the effective surface area of the electrode must generally be increased. We explored the effect of plasma treatment on the surface wettability of MWCNT. With a steam–plasma treatment the surface of MWCNT becomes converted from superhydrophobic to superhydrophilic; this hydrophilic property is attributed to –OH bonding on the surface of MWCNT. We reported the synthesis at 400 °C of MWCNT on nickel–titanium multilayered metal catalysts by thermal chemical vapor deposition. Applying plasma with a power less than 25 W for 10 s improved the electrochemical and biological properties, and circumvented the limitation of the surface reverting to a hydrophobic condition; a hydrophilic state is maintained for at least one month. The MEA was used to record neural signals of a lateral giant cell from an American crayfish. The response amplitude of the action potential was about 275 μV with 1 ms period; the recorded data had a ratio of signal to noise up to 40.12 dB. The improved performance of the electrode makes feasible the separation of neural signals and the recognition of their distinct shapes. With further development the rapid treatment will be useful for long-term recording applications.

(Some figures in this article are in colour only in the electronic version)

1. Introduction

A fundamental objective of neuroscience is to develop quantitative descriptions of functional operations and their coordination within a neuron that enable it to function as an integrated unit to process information. The communication of information among neurons, or between neuron and muscle, requires a signal to travel some distance. Through electrical stimulation applied to nerves and muscles, electrophysiologists

[7] Author to whom any correspondence should be addressed.

demonstrated that a command from the brain to a muscle to generate a movement is mediated by the flow of an electric current along nerve fibers, a so-called action potential (AP) [1]. Hodgkin and Huxley demonstrated that axons at rest are electrically polarized, exhibiting a resting potential of approximately −60 mV across a membrane [2]. This AP propagates along the length of the axon through a local depolarization of each neighboring patch of membrane, causing that patch to also generate an AP. With the decreasing size of a microelectrode, its impedance increases and the charge-transfer capability decreases; a large impedance decreases the ratio of the signal of the AP to noise. Decreasing the impedance generally requires increasing the effective surface area of the electrode.

Carbon nanotubes (CNT) exhibit intrinsically large surface areas (700–1000 $m^2\ g^{-1}$) [3], high mechanical strength (>1 TPa) [4], high electrical conductivity and intriguing physicochemical properties [5–7]. The extraordinary strength, toughness, electrical conductivity and surface area of multi-walled carbon nanotubes (MWCNT) make them attractive for interfacing with neural systems to develop biocompatible, durable and robust neuroprosthetic devices [8]. Hence, CNT have become an attractive material for neuro-electronic interfaces [9–11]. By growing CNT on microelectrodes, the nanostructure of the CNT inherently increases the effective interfacial area between the microelectrode and neuron [12–14]. CNT have also been demonstrated to be a biocompatible substrate that promotes neural growth, boosts neural activity [9] and transmits electrical stimulation [11, 14]. Other applications include a multifunctional carbon nanopipette (CNP) that facilitates cellular measurements because of its small size, which enables interrogation of organelles within living cells in a minimally invasive fashion [15–19]. These promising results have led to the fabrication of CNT into microelectrodes or even microprobes for neural recording and stimulation. Besides, using different nanostructures to record neuron signals such as Lieber's group presented arrays of nanowire field-effect transistors integrated with the individual axons and dendrites of live mammalian neurons, where each nanoscale junction can be used for spatially resolved, highly sensitive detection, stimulation and/or inhibition of neuronal signal propagation [20]. Yoon's group have fabricated a heterostructured IrO_2/Au nanowire on a flexible needle probe providing low impedance and high charge storage capacity, which can enhance neural sensing and stimulating efficiency [21].

Microelectrode arrays (MEA) based on MWCNT have been fabricated for neuroscience applications, and the effect of plasma treatment on the surface wettability of MWCNT has been explored. A steam–plasma (SP) treatment serves to modify the surface of MWCNT from superhydrophobic to superhydrophilic; the hydrophilic property is attributed to –OH bonds on the surface of the MWCNT. Among achievements related to these devices are the use of a micro-multi-probe electrode array to measure neuron signals with silicon-on-insulator (SOI) technology [22], a synthesis at 400 °C of MWCNT on nickel–titanium (Ni/Ti) multilayered metal catalysts by thermal chemical vapor deposition (CVD) [23] and improving the adhesion of MWCNT to a substrate with a microwave treatment [24]. Gabay's microelectrodes were fabricated as dense islands of MWCNT on lithographically defined conductors of passivated titanium nitride on a silicon dioxide (SiO_2) substrate [13]. A novel hydrophilic method to improve on the results of Gabay's group involved MEA as grown based on MWCNT; this method differs from that of the Li group in the modification by oxygen (O_2) reactive-ion etching (RIE) [25]. The degree of modification of the surface wettability of the film was controlled by the rate of flow of gaseous O_2 during the RIE. Wang's group reported an adsorption treatment involving noncovalent binding of molecules [12]; the amphiphilic poly(ethylene glycol)–lipid conjugates (PEG–PL) bind to CNT via van der Waals and hydrophobic interactions between the two lipid alkyl chains and the nanotube sidewall [26, 27], so that the CNT microelectrodes became more hydrophilic. In Meyyappan's fabrication, a thin polypyrrole (PPy) coating greatly increased the mechanical strength of the CNT and enabled them to maintain a free-standing structure [28, 29]. We applied the SP treatment to modify the surface of MWCNT from superhydrophobic to superhydrophilic. A treatment with plasma power under 25 W for 10 s much improves the electrochemical and biological properties, and we overcame the limitation of the surface reverting to a hydrophobic condition so that a hydrophilic state is maintained for at least one month.

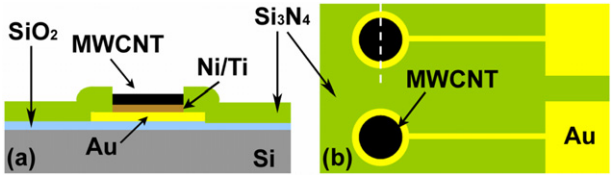

Figure 1. Schematic of MEA based on MWCNT. (a) Cross-sectional view. (b) Top view of the electrode scheme.

2. Experiments

2.1. MEMS fabrication

The experimental method consisted of three main steps—MEMS fabrication, growth of MWCNT and their treatment. We applied MEMS technology to develop the fabrication of MEA based on MWCNT, beginning with a general silicon wafer (φ: 100 mm, ρ: 1–100 Ω cm). Lithography, CVD, dry etching and physical vapor deposition were used to develop the MEA. Figure 1 shows a schematic view of the MEA based on MWCNT.

The fabrication begins with (a) RCA standard cleaning served to remove particles and ion contamination, (b) a SiO_2 film (wet-oxide type, thickness 500 nm) grown as an isolating layer and (c) patterning of electrodes with a lift-off method. The gold (Au, thickness 100 nm) and Ti were evaporated with an E-beam vacuum evaporator; the Ti layer (thickness 20 nm) provides adhesion. The metal electrodes and traces were defined when the sacrificial layer of photoresist was washed

away in an ultrasonic bath in acetone. The materials on top were lifted off and washed together with the photoresist below. After the lift-off, the Au/Ti remained only in the regions where it had direct contact with the substrate. The trace was defined to have width 5 μm and thickness 120 nm. (d) A silicon nitride (Si_3N_4) layer (thickness 2 μm) was deposited on top of the entire wafer as a passivation dielectric layer using plasma-enhanced chemical vapor deposition (PECVD). Si_3N_4 exhibits a relative permittivity ($\varepsilon_r = 7.5$) greater than that of SiO_2 ($\varepsilon_r = 4$), so as to block ion transport efficiently. Its conformal surface is easily patterned, impermeable to ions, biocompatible and attractive for cellular attachment. A 2 μm Si_3N_4 layer is adequate for AP measurements and blocks ion transport through the passivation capacitance. (e) Via holes of electrodes and contact pads were opened to the Au layer using RIE. (f) The catalyst layer of Ni (thickness 5 nm) and the under layer of Ti (thickness 20 nm) were formed with an E-beam vacuum evaporator and patterned with a lift-off method.

2.2. Growth and treatment of MWCNT

(a) MWCNT were synthesized on Ni/Ti multilayered metal catalysts by thermal CVD at 400 °C, using acetylene as a source of carbon in a quartz tube furnace (diameter 75 mm). The Ni/Ti multilayered metal catalysts effectively decreased the temperature to grow CNT; we used a temperature ramp to 400 °C at a rate of 20 °C min^{-1} and a constant flow of argon of about 100 sccm (standard cm^3 min^{-1}). At the stable temperature, acetylene (60 sccm) and hydrogen (10 sccm) were added to the furnace for 15 min. The chip cooled at a rate 5 °C min^{-1}.

(b) MWCNT as grown were placed on a capacitance-coupled electrode driven at radio frequency (RF); the RF power was set at 25 W, 50 W and 75 W, respectively, and the working pressure in the chamber was about 20 Pa. Distilled water was heated on a hotplate at 120 °C to produce steam that flowed into the plasma chamber during the surface treatment; the rate of flow of steam was set at 1 sccm with durations 10, 30 and 60 s, respectively.

3. Results and discussion

3.1. Images from a scanning electron microscope (SEM)

The MWCNT as grown were synthesized on Ni/Ti multi-layered metal catalysts on a silicon substrate, and the SP RIE served to treat the wetting properties of the surface. Figures 2(a) and (b) show the morphologies of treated MWCNT (25 W, 10 s) were not different from those as grown. Figure 2 show SEM (JEOL, JSM-6500) images of MEA based on MWCNT. The chip consisted of 1 × 4 microelectrode arrays with four neural recording channels. The MWCNT electrode (φ: 57 μm) on a conductive Au pad was patterned on the SiO_2 substrate. The open size of the electrode is 2500 μm^2 with 500 μm intervals. We have damaged the MWCNT electrodes manually to get the cross-section view shown in figure 2(a). The length of the CNTs determined by using the SEM software, which showed that one of the functions can be used to compute the distance between two points. The MWCNT had length about 1.6 μm and diameter about 20 nm, yielding an aspect ratio greater than 70. We used wire bonding to connect bonding pads to the printed-circuit board. The aluminum (Al, diameter 25 μm) wire was used in the wedge wire bonding. The substrate and electrical traces were packaged appropriately with biocompatible epoxy (Epoxy Technology, EPO-TEK 301-2) that has United States Pharmacopeia (USP) biocompatibility in Class VI.

Besides, to modify the MWCNT surface wettability from superhydrophobic to superhydrophilic, a series of experiments were conducted by varying the plasma process parameters. Figure 2(c) shows the SEM morphologies of MWCNT after SP treatment for 10, 30 and 60 s at 25 W, 50 W and 75 W, respectively. It can be observed that the morphologies and structures of MWCNT deteriorate with the increase of SP power and duration treatment. It indicates that the deterioration of MWCNT morphology and structure is negligible after SP treatment for 10 s at 25 W. The difference in the morphologies and structures only can be clearly observed at a higher plasma power and long duration treatment.

3.2. Raman spectra

Micro-Raman spectra (Horiba Jobin Yvon HR-800, laser excitation wavelength: 633 nm) were also used to measure the degree of graphitization for CNT. The D-band intensity is defect-induced (1350 cm^{-1}) and the G-band intensity is a graphite-related optical mode (1550–1605 cm^{-1}) [30]. The G-band to D-band intensity ratio (I_G/I_D, G/D ratio) corresponds to the graphitization of CNT, which can be used as an indication of the CNT quality. A higher I_G/I_D ratio means better graphitization of CNT. A lower I_G/I_D ratio indicates more defects and amorphous carbon in CNT [31].

Raman spectra were used to characterize the graphitization of MWCNT as grown, as well as those after SP treatment for 10, 30 and 60 s at 25 W, 50 W and 75 W, respectively, as shown in figure 3(a). The impact of graphitization due to SP treatment can be observed. Figure 3(b) shows the G/D ratio, I_G/I_D, of the Raman spectra versus SP treatment time at different powers. I_G/I_D for MWCNT as grown is 0.42. The ratio decreased slightly as the SP treatment time increased from 10 s ($I_G/I_D = 0.4$) to 60 s ($I_G/I_D = 0.38$) at 25 W, and the ratio decreased obviously as the SP treatment time increased from 10 s ($I_G/I_D = 0.37$) to 60 s ($I_G/I_D = 0.31$) at 75 W. The lower I_G/I_D ratio indicates a lower degree of graphitization for SP-treated MWCNT. These results reveal that the graphitization of MWCNT was slightly damaged after SP treatment for 10 s at 25 W. This indicates that SP treatment may lead to slight degradation of MWCNT performance like sp^2-hybridized C=C graphite, but to large enhancement of the hydrophilic wetting property of MWCNT. Based on SEM Raman spectra analyses, the SP treatment for 10 s at 25 W is the optimized process recipe for enhancing the hydrophilic wetting property of MWCNT.

3.3. X-ray photoelectron spectroscopy (XPS)

XPS (Ulvac-PHI, PHI 1600) analyses were performed to investigate the changes of chemical concentration on MWCNT.

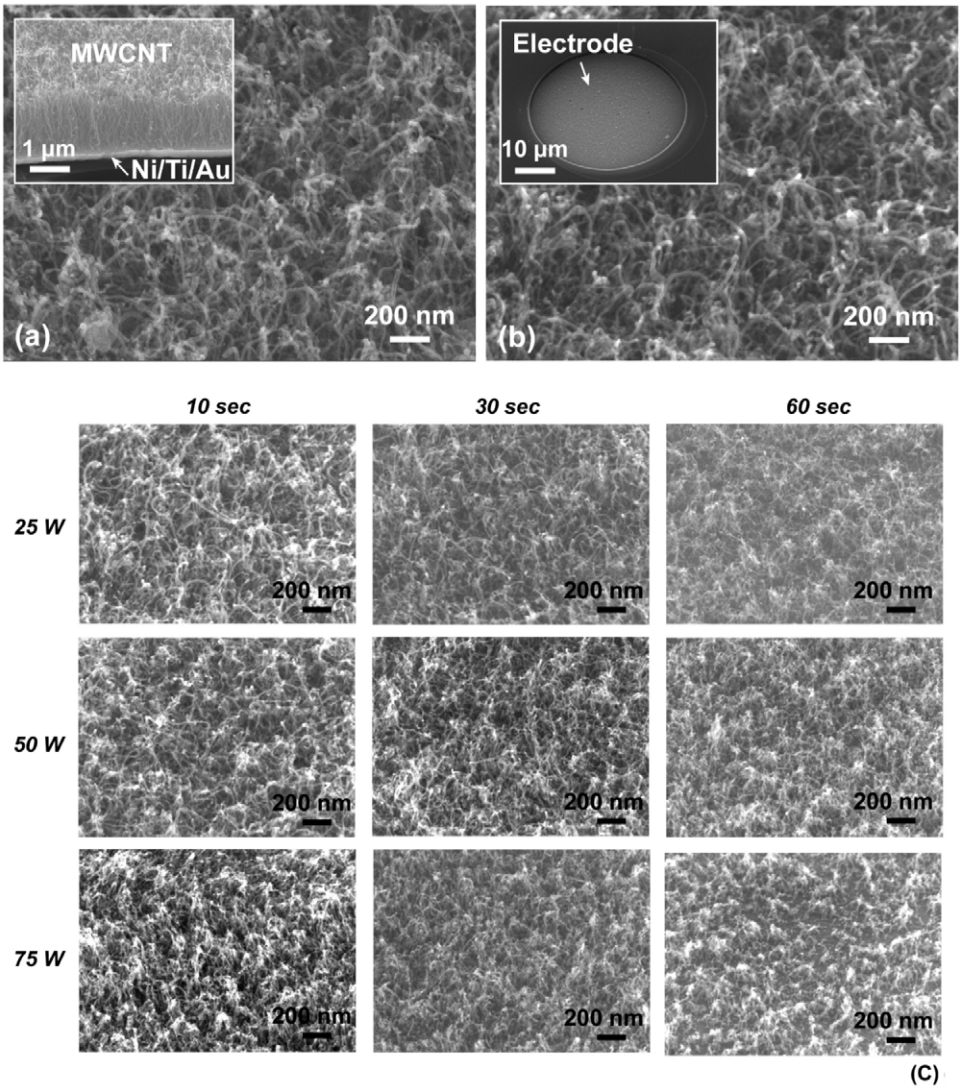

Figure 2. SEM images of MEA based on MWCNT. (a) MWCNT as grown were synthesized at 400 °C, and a side-view image of an MWCNT film. (b) Morphologies of MWCNT after SP treatment (25 W, 10 s) and a top-view image of an MWCNT electrode. (c) The morphologies of MWCNT after SP treatment for 10, 30 and 60 s at 25 W, 50 W and 75 W, respectively.

A broad survey scan should be obtained first to identify the elements present. Energy peaks in the survey scan identify the elemental composition of the uppermost 20–50 Å of the analyzed surface. All elements, except hydrogen and helium, are detected. The survey scans of MWCNT as grown and treated with SP are shown in figure 4(a). The appearance of the smaller C and larger O peaks in the XPS survey spectrum for MWCNT modified with SP, compared to that of as grown, clearly indicates the bonding of O and OH chains onto the resultant MWCNT as grown.

The Gaussian decomposition of the peaks of MWCNT as grown and treated with SP respectively is shown in figures 4(b) and (c). Both MWCNT as grown and treated exhibit five peaks at 284.4, 285.5, 286.7, 287.9 and 289.5 eV which are attributed to sp^2-hybridized C=C graphite, sp^3-hybridized C–C diamond-like, C–OH, C=O and OH–C=O bonds, respectively [25, 32, 33]. The relative percentages of C–OH, C=O and OH–C=O bonds for MWCNT treated with 25 W-10 s SP (C–OH 17.7%; C=O 11%; OH–C=O 5.5%) are higher than those of MWCNT as grown (C–OH 8.6%; C=O 2.3%; OH–C=O 0.7%). It is probable that the formation of hydrophilic chemical bonds such as C–OH, C=O and OH–C=O on the MWCNT surface was enhanced by 25 W-10 s SP treatment.

3.4. Wettability of surfaces

After the SP RIE treatment, the wetting properties of surfaces were investigated by means of measurements of the contact angle. A droplet (distilled water, 2 μl) was dropped onto the surface of MWCNT. Images of the droplets were captured with a charged-coupled-device (CCD) camera. The MWCNT as grown are superhydrophobic with a measured average contact angle as large as 152° ($n = 3$). Treatment with an SP for a specific duration was utilized to modify the wettability of the MWCNT. On increasing the duration of treatment of the MWCNT from 10 to 30 s and finally to 60 s, the superhydrophilic wetting property was observed through

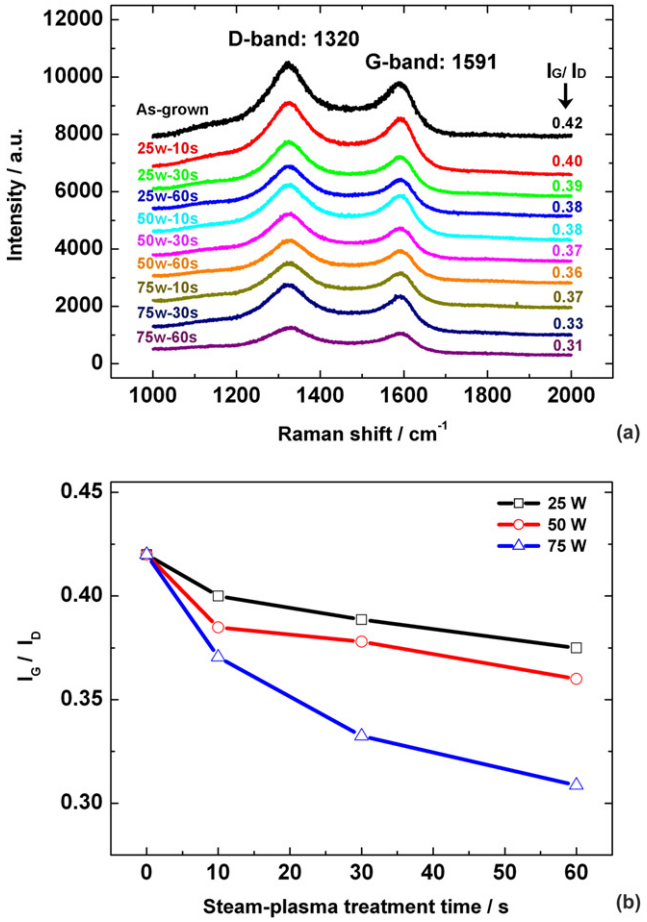

Figure 3. Raman spectra data. (a) The Raman spectra of MWCNT as grown and SP treatment for 10, 30 and 60 s at 25, 50 and 75 W. (b) The trend chart of G/D ratio (I_G/I_D) versus SP treatment time and power.

spreading of the distilled water droplet on the surface. The surface of MWCNT treated with SP is superhydrophilic, with a measured average contact angle as small as 5° ($n = 3$). Figure 5(a) presents a trend chart to show the variation of contact angles with duration of SP treatment. Treating surfaces in this way makes them more hydrophilic than with oxygen RIE treatment [25]. In a long-term recording experiment, the chips must be immersed in phosphate-buffered saline (PBS, 0.01 M, pH = 7.4, comprising NaCl, KCl and buffer); the temperature should remain at 37 °C to simulate the necessary conditions of the environment of a cell incubator. After one month, the hydrophilic state was maintained, as shown in figure 5(b) (contact angle data <8°, $n = 3$). Furthermore, with increasing time, the contact angle of MWCNT as grown decreases from 152° to 54°. The hydrophobic-to-hydrophilic transition was attributed to nonspecific adsorption of proteins in the medium to the CNT surface [12, 34].

3.5. Cyclic voltammetry (CV)

As the most widely used technique to acquire qualitative information about electrochemical reactions, CV rapidly provides information about the thermodynamics of oxidation processes, the kinetics of heterogeneous electron-transfer reactions and coupled chemical reactions or adsorptive processes. CV consists of scanning linearly the potential of a stationary working electrode using a triangular potential waveform. Depending on the information sought, single or multiple cycles are applied; the resulting plot of current versus potential is termed a cyclic voltammogram [35]. We used a CV instrument (CH Instruments, CHI 760B) to measure the electrochemical properties of the developed MEA in a two-electrode cell, with the MWCNT electrode as working electrode and a large silver–silver chloride electrode (Ag/AgCl) as reference electrode. The current difference (Δi) between the positive and negative potential cycles corresponds to the sum of the charging and discharging currents at the electrode and electrolyte interface, which is expected to exhibit a linear dependence corresponding to a DC capacitance (C) under a fixed scan rate:

$$\Delta i = C \cdot \upsilon. \tag{1}$$

Figure 6 shows a CV of MWCNT in PBS (0.01 M, pH = 7.4, 27 °C) with scan rate 500 mV s^{-1}. Normalizing the obtained capacitance with the area of the electrode yields a large DC specific capacitance that increased from 0.54 to 2.25 mF cm^{-2} after treatment. The measured value is greater than that of a conventional noble metal microelectrode (Au, ~10 μF cm^{-2}) at the same physical size.

3.6. Electrochemical impedance spectroscopy

The impedance at the electrode–electrolyte interface influences the ability to record neural signals. Increasing the impedance of an electrode decreases the transmitted electric current and increases the noise, so as to influence the ratio of signal to noise (SNR) of the spike. Electrochemical impedance spectra (EIS), based largely on methods to analyze circuits in electrical engineering practice, were developed by Sluyters and co-workers and extended by others [36]. To exhibit the electrochemical behavior of the developed MEA, we used EIS to measure the impedance and phase between MWCNT and a reference electrode. EIS depict the variation of total impedance in the complex plane. The measured total impedance of the cell, Z, is expressed as a combination of resistance and capacitance in series; these two elements provide the real and imaginary components of impedance. In the experiment, the impedance data were obtained on immersing the recording site in PBS (0.01 M, pH = 7.4, 27 °C) bio-electrolyte. The test signal from EIS (CH Instruments, CHI 760B) had a sinusoidal form (AC wave, 10 mV; frequencies 0.1–10 kHz) with respect to a conventional Ag/AgCl reference electrode. Figure 7(a) shows the interface impedance of MWCNT measured with EIS immediately. For a typical electrode with open area 2500 μm^2 immersed in PBS, the impedance decreased from 51.2 to 3.49 kΩ at 1 kHz (nerve working frequency) after SP treatment. The impedance of the treated MWCNT is much smaller than that from other materials, such as Au, Pt and Ir electrodes (Au, 2500 μm^2, 335.6 kΩ at 1 kHz); the Au and Pt

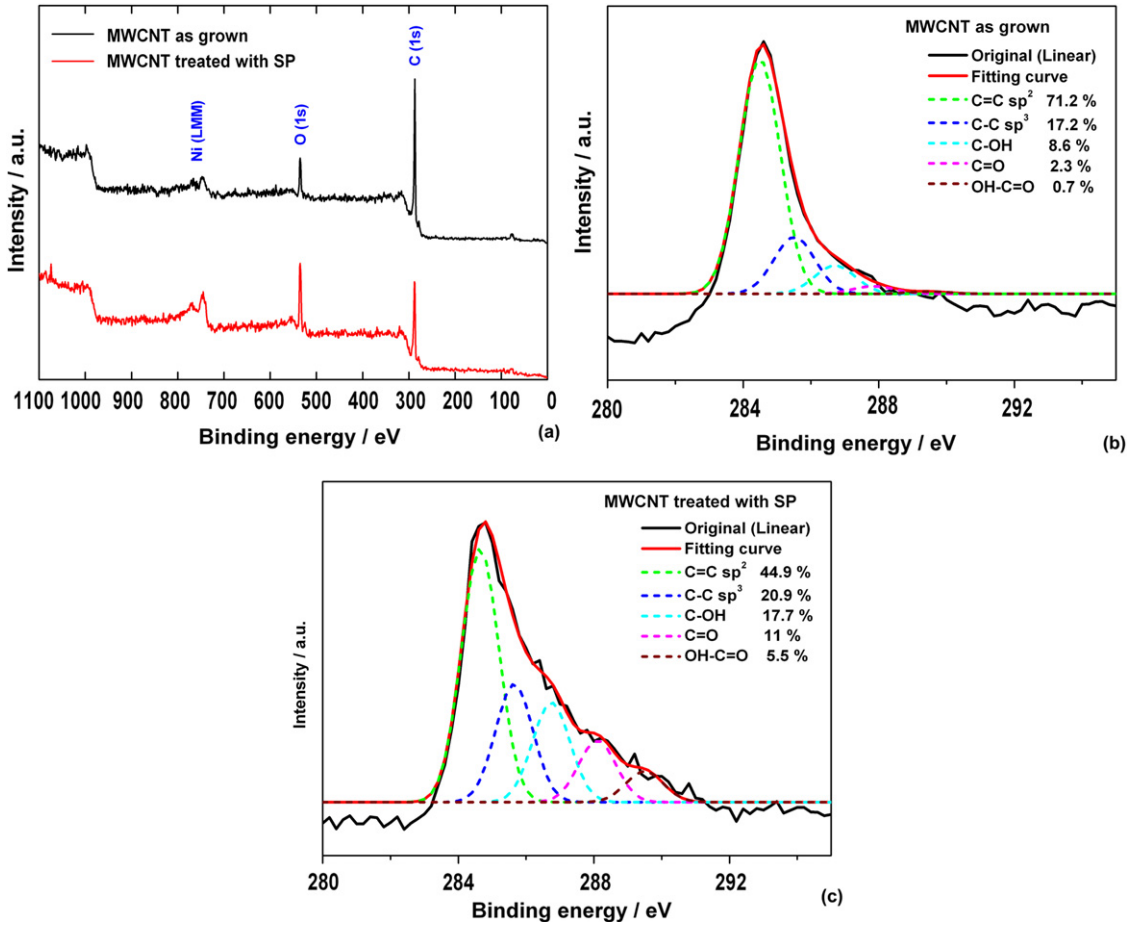

Figure 4. XPS data of MWCNT as grown and treated. (a) Wide scan survey spectra. (b) Gaussian decompositions of C 1s spectra of MWCNT as grown. (c) Gaussian decompositions of C 1s spectra of MWCNT treated with 25 W for 10 s SP.

electrode interfaces are highly polarized [37]. When the value was normalized to the same geometric area (10 000 μm^2), the impedance of the treated MWCNT (0.87 kΩ at 1 kHz) is much smaller than in other literature [13, 38]. Figure 7(b) shows the Nyquist plot showing an impedance spectrum for a treated MWCNT electrode in the frequency range 0.1–10 kHz. The data represent a constant phase-element (CPE) interface [39–44]. The CPE deviates from a capacitance with impedance defined as

$$Z = 1/Y_0(j2\pi f)^{\alpha} \tag{2}$$

in which f denotes frequency/Hz, with Y_0 and α fitting parameters. The fit yields $\alpha = 0.89$, near the value of an ideal capacitor for which $\alpha = 1$. The physical explanation is that the CPE behavior reflects the roughness of the electrode that resembles a 3D porous structure. Another explanation involves inhomogeneous reaction rates on a surface. On immersion in PBS solution, the long-term stability of the neural probe was tested by means of an impedance measurement. The Si_3N_4 film adhered to the chip satisfactorily after one month; the adhesion remained tight with no discernible degradation and the variation of the interface impedance was less than 1% over that duration.

3.7. Recording neural signals

Biocompatibility is an important criterion for biological applications. For MWCNT grown on an Ni/Ti/Au substrate, there are reports that Ni is cytotoxic, releasing harmful Ni ions and causing cell death [45]. However, the thickness of Ni used as a catalyst for MWCNT growth is several nanometers. This layer becomes nanoparticles encapsulated by MWCNT after thermal CVD. In addition, the mechanism of MWCNT growth employs the 'base growth' mechanism with the Ni nanoparticles under dense MWCNT. Release of Ni ions from the bottom layer to cells will be reduced. Despite previous reports about the toxicity of Ni, several groups have demonstrated the high viability of a cell culture on MWCNT as grown using Ni as a catalyst [13, 46]. Furthermore, a Ti layer was added with the Ni layer to form an Ni–Ti alloy, which has good biocompatibility [47, 48]. Based on the above reasons, the MWCNT electrodes with Ni/Ti/Au substrates may be usable for biological applications, such as implanted neural probes. Additionally, the MWCNT electrodes developed in this work could be applied to potential applications with less concern about toxicity.

To confirm the functionality of the electrode, we measured the neural signal of the escape circuit of American crayfish

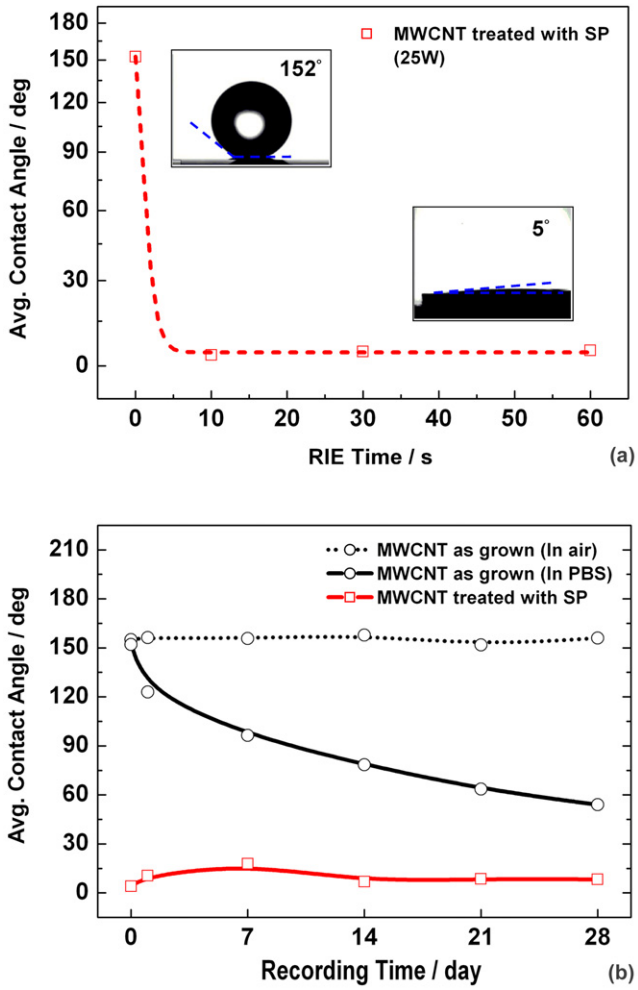

Figure 5. Trend charts of the variation of contact angle. (a) With duration of SP treatment time. (b) For long-term (one month) recording, respectively ($n = 3$).

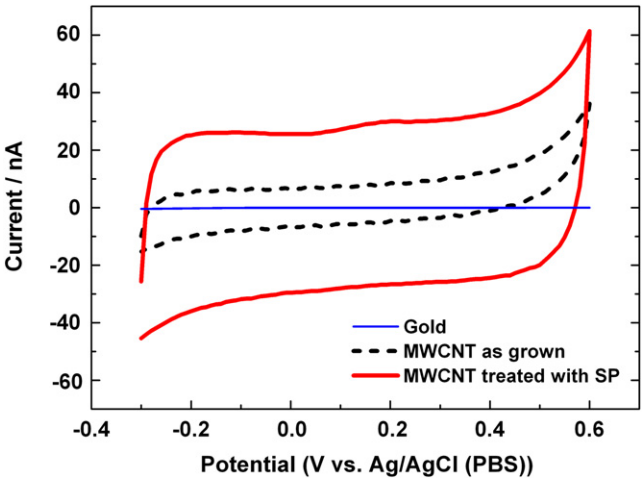

Figure 6. CV of two types of MWCNT in PBS (scanning rate 500 mV s^{1}).

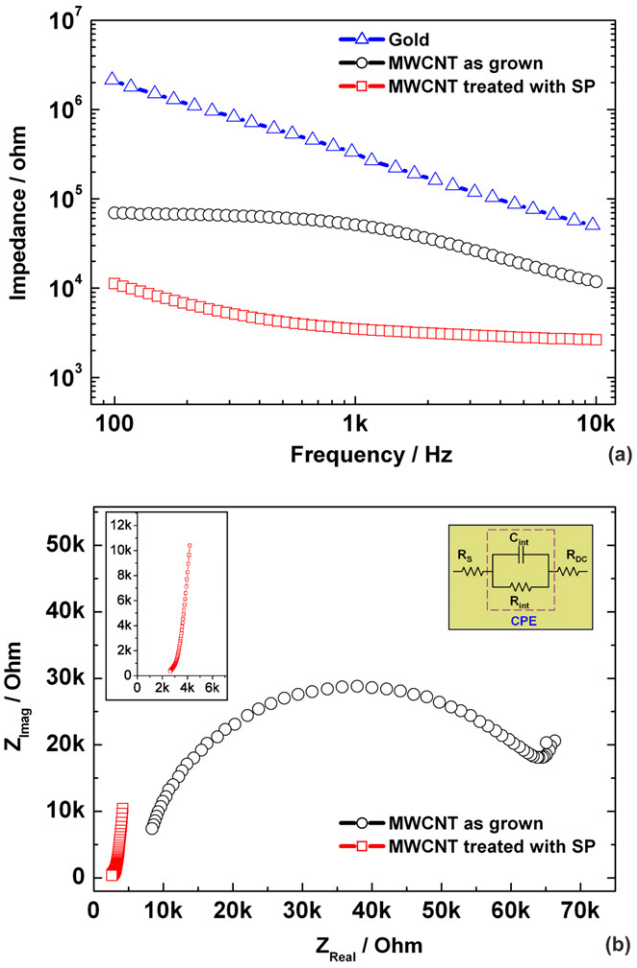

Figure 7. Electrochemical impedance spectroscopy data of MWCNT electrode immersed in PBS (0.01 M, 27 °C). (a) The impedance magnitude decreased from 51.2 to 3.49 kΩ at 1 kHz after SP treatment. (b) Nyquist plot of MWCNT as grown and treated (alternating current sinusoidal waves, 10 mV; frequencies 0.1–10 kHz). Data fitted to an equivalent circuit model shown in the inset.

with the developed neural probe. The advantage of the escape circuit from a crayfish is the large diameter of an axon and the simple structure: the diameter of an axon is greater than 10 μm and the length about 1 mm. The neuron is large enough for contact with a microelectrode, to minimize the distance between the electrode and the measured neuron cell. A schematic view of the electrophysiology system, which was used to record the neuron signal from the microelectrode, appears in figure 8(a).

From juvenile crayfish kept in an aquarium near 23 °C, we selected junior crayfish (length 2–5 cm) for our experiments. After 10 min on ice the crayfish lost the ability to move. The crayfish was pinned in a dish filled with van Harreveld's solution [49]. The abdominal nerve cord of the escape circuits was exposed dorsally on removing the exoskeleton and separating the phasic flexor musculature using an isolated abdomen preparation [50]. Figure 8(b) shows the experimental set-up. In the escape circuits of the crayfish, the mechanosensory primary afferents received an environmental excitation. Part of the neural signal transmits directly to the lateral giant (LG) nerve fiber through the electrical synapses. Pairs of silver wires were placed on the mechanosensory

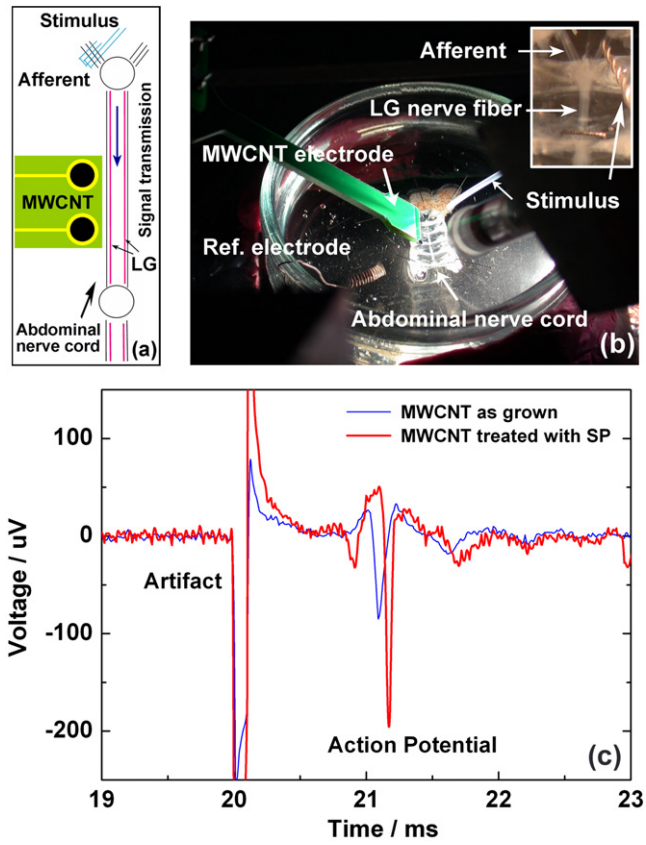

Figure 8. Extracellular recording from an LG nerve fiber. (a) Schematic view of recording system. (b) Overview of a complete electrophysiology recording system for a crayfish. (c) Extracellular signal with large SNR was obtained from an LG nerve fiber using MEA based on MWCNT and treated with SP, compared with MWCNT as grown.

primary afferent neurons for stimulation. The functions of the electrophysiology system were divided into two parts—one for electrical stimulation and the other for recording. The electrical stimulation was produced with a digital-to-analog converter card and amplifier circuits. The amplitude and frequency of the input voltage were controlled with software in a computer. The recorded signal was amplified with a commercial amplifier.

In the extracellular neural recording, figure 8(c) shows the signal from the LG nerve fiber with the MWCNT electrode placed on the dorsal side of the nerve cord by electrical shocking on the tailfin afferents. After alternating, the square waveform of a shock voltage was about ± 1 V with period 0.2 ms, and the responsive amplitude (peak to peak) of the AP recorded with the treated MWCNT electrode which was about 275 μV with period 1 ms; the recorded data were marked with an SNR up to 40.12 dB. This SNR is defined as the quotient of the peak-to-peak value of the spike and the root mean square of the noise [51]. For data recorded with MEA based on MWCNT as grown, a smaller SNR, 24.69 dB, was obtained under the same conditions, or 0.61 of the ratio for the treated MWCNT electrode. By these measurements the results demonstrate the recording ability of MEA based on MWCNT; with the enhanced performance of the MWCNT, it becomes feasible to separate neural signals and to recognize their distinct shapes.

4. Conclusion

To decrease the impedance of MEA, we fabricated and treated the MEA based on MWCNT for neuroscience applications. The MWCNT were synthesized on Ni/Ti multilayered metal catalysts at 400 °C by thermal CVD; these catalysts effectively decreased the CNT growth temperature. We also demonstrated the effect of SP treatment on the surface wettability of MWCNT.

The results show not only that the surface of MWCNT can be modified from hydrophobic to hydrophilic, but also that the electrode yields a large DC specific capacitance and a decreased AC impedance at the interface of MWCNT in PBS after SP treatment. In extracellular recording, the AP was recorded with the treated MWCNT; the SNR was up to 40.12 dB. For data recorded with MEA based on MWCNT as grown, a smaller SNR, 24.69 dB, was obtained under the same conditions, or 0.61 of the ratio for the treated MWCNT electrode. With the treated MWCNT, it becomes feasible to separate neural signals and to recognize their distinct shapes. This work provides opportunities to modify CNT characteristics suitable for CMOS interconnects and biological applications. Continued improvement of SNR of the neural signal would be important for a multiple-electrode measurement system. Future durability tests must include a toxicity test, long-term signal recording and stimulation in neural cells.

Acknowledgments

The National Science Council of the Republic of China (Taiwan) provided partial support (grant 96-2627-E-007-002). We thank Professor Fan-Gang Tseng of the National Tsing Hua University for providing the fabrication facilities and impedance measurement.

References

[1] Brazier M A B 1988 *A History of Neurophysiology in the 19th Century* (New York: Raven Press)
[2] Hodgkin A L and Huxley A F 1939 Action potentials recorded from inside a nerve fibre *Nature* **144** 710–1
[3] Li J, Ng H T, Cassell A, Fan W, Chen H, Ye Q, Koehne J, Han J and Meyyappan M 2003 Carbon nanotube nanoelectrode array for ultrasensitive DNA detection *Nano Lett.* **3** 597–602
[4] Krishnan A, Dujardin E, Ebbesen T W, Yianilos P N and Treacy M M J 1998 Young's modulus of single-walled nanotubes *Phys. Rev.* B **58** 14013–9
[5] Gooding J J 2005 Nanostructuring electrodes with carbon nanotubes: a review on electrochemistry and applications for sensing *Electrochim. Acta* **50** 3049–60
[6] Musameh M, Lawrence N S and Wang J 2005 Electrochemical activation of carbon nanotubes *Electrochem. Commun.* **7** 14–8
[7] Shanmugam S and Gedanken A 2006 Electrochemical properties of bamboo-shaped multiwalled carbon nanotubes generated by solid state pyrolysis *Electrochem. Commun.* **8** 1099–105

[8] Kotov N A *et al* 2009 Nanomaterials for neural interfaces *Adv. Mater.* **21** 3970–4004

[9] Lovat V, Pantarotto D, Lagostena L, Cacciari B, Grandolfo M, Righi M, Spalluto G, Prato M and Ballerini L 2005 Carbon nanotube substrates boost neuronal electrical signaling *Nano Lett.* **5** 1107–10

[10] Gheith M K, Pappas T C, Liopo A V, Sinani V A, Shim B S, Motamedi M, Wicksted J P and Kotov N A 2006 Stimulation of neural cells by lateral currents in conductive layer-by-layer films of single-walled carbon nanotubes *Adv. Mater.* **18** 2975–9

[11] Mazzatenta A, Giugliano M, Campidelli S, Gambazzi L, Businaro L, Markram H, Prato M and Ballerini L 2007 Interfacing neurons with carbon nanotubes: electrical signal transfer and synaptic stimulation in cultured brain circuits *J. Neurosci.* **27** 6931–6

[12] Wang K, Fishman H A, Dai H and Harris J S 2006 Neural stimulation with a carbon nanotube microelectrode array *Nano Lett.* **6** 2043–8

[13] Gabay T, Ben-David M, Kalifa I, Sorkin R, Abrams Z R, Ben-Jacob E and Hanein Y 2007 Electro-chemical and biological properties of carbon nanotube based multi-electrode arrays *Nanotechnology* **18** 1–6

[14] Keefer E W, Botterman B R, Romero M I, Rossi A F and Gross G W 2008 Carbon nanotube coating improves neuronal recordings *Nat. Nanotechnol.* **3** 434–9

[15] Kim B M, Murray T and Bau H H 2005 The fabrication of integrated carbon pipes with sub-micron diameters *Nanotechnology* **16** 1317–20

[16] Freedman J R, Mattia D, Korneva G, Gogotsi Y, Friedman G and Fontecchio A K 2007 Magnetically assembled carbon nanotube tipped pipettes *Appl. Phys. Lett.* **90** 103108

[17] Schrlau M G, Brailoiu E, Patel S, Gogotsi Y, Dun N J and Bau H H 2008 Carbon nanopipettes characterize calcium release pathways in breast cancer cells *Nanotechnology* **19** 325102

[18] Schrlau M G, Falls E M, Ziober B L and Bau H H 2008 Carbon nanopipettes for cell probes and intracellular injection *Nanotechnology* **19** 015101

[19] Singhal R, Bhattacharyya S, Orynbayeva Z, Vitol E, Friedman G and Gogotsi Y 2010 Small diameter carbon nanopipettes *Nanotechnology* **21** 015304

[20] Patolsky F, Timko B P, Yu G, Fang Y, Greytak A B, Zheng G and Lieber C M 2006 Detection, stimulation, and inhibition of neuronal signals with high-density nanowire transistor arrays *Science* **313** 1100–4

[21] Yoon H, Hankins P, Oh S, Harbaugh R E and Varadan V K 2010 Heterostructured IrO_2/Au nanowire electrodes and unit recordings from Hippocampal Rat Brain *J. Nanotechnol. Eng. Med.* **1** 021006

[22] Chen C H, Yao D J, Tseng S H, Lu S W, Chiao C C and Yeh S R 2009 Micro multi-probes electrode array to measure neuron signals *Biosens. Bioelectron.* **24** 1911–17

[23] Su H C, Chen C H, Chen Y C, Yao D J and Yew T R 2008 Low temperature synthesis of multi-walled carbon nanotubes *NT08 (Montpellier)* p 142

[24] Su H C, Chen C H, Chen Y C, Yao D J, Chen H, Chang Y C and Yew T R 2010 Improving the adhesion of carbon nanotubes to a substrate using microwave treatment *Carbon* **48** 805–12

[25] Li P, Lim X, Zhu Y, Yu T, Ong C K, Shen Z, Wee A and Sow C H 2007 Tailoring wettability change on aligned and patterned carbon nanotube films for selective assembly *J. Phys. Chem.* B **111** 1672–8

[26] Kam N W S, Liu Z and Dai H 2005 Functionalization of carbon nanotubes via ceavable disulfide bonds for efficient intracellular delivery of siRNA and potent gene silencing *J. Am. Chem. Soc.* **127** 12492–3

[27] Kam N W S, O'Connell M, Wisdom J A and Dai H 2005 Carbon nanotubes as multifunctional biological transporters and near-infrared agents for selective cancer cell destruction *Proc. Natl Acad. Sci.* **102** 11600–5

[28] Meyyappan M, Barbara Nguyen-Vu T D, Chen H, Cassell A M, Andrews R and Li J 2006 Vertically aligned carbon nanofiber arrays: an advance toward electrical–neural interfaces *Small* **2** 89–94

[29] Wang J, Xu Y, Chen X and Sun X 2007 Capacitance properties of single wall carbon nanotube/polypyrrole composite films *Compos. Sci. Technol.* **67** 2981–5

[30] Dresselhaus M S, Dresselhaus G, Jorio A, Filho A G S and Saito R 2002 Raman spectroscopy on isolated single wall carbon nanotubes *Carbon* **40** 2043–61

[31] Endo M, Kim Y A, Fukai Y, Hayashi T, Terrones M, Terrones H and Dresselhaus M S 2001 Comparison study of semi-crystalline and highly crystalline multiwalled carbon nanotubes *Appl. Phys. Lett.* **79** 1531–3

[32] Kovtyukhova N I, Mallouk T E, Pan L and Dickey E C 2003 Individual single-walled nanotubes and hydrogels made by oxidative exfoliation of carbon nanotube ropes *J. Am. Chem. Soc.* **125** 9761–9

[33] Yu D and Dai L 2009 Self-assembled graphene/carbon nanotube hybrid films for supercapacitors *J. Phys. Chem. Lett.* **1** 467–70

[34] Yeh S R *et al* 2009 Interfacing neurons both extracellularly and intracellularly using carbon-nanotube probes with long-term endurance *Langmuir* **25** 7718–24

[35] Wang J 2000 *Analytical Electrochemistry* (New York: Wiley)

[36] Bard A J and Faulkner L R 2001 *Electrochemical Methods: Fundamentals and Applications* (New York: Wiley)

[37] Fricke H 1932 The theory of electrolytic polarization *Phil. Mag.* **14** 310–8

[38] Paik S J, Park Y and Cho D I D 2003 Roughened polysilicon for low impedance microelectrodes in neural probes *J. Micromech. Microeng.* **13** 373–9

[39] Li J, Koehne J E, Cassell A M, Chen H, Ng H T, Ye Q, Fan W, Han J and Meyyappan M 2004 Inlaid multi-walled carbon nanotube nanoelectrode arrays for electroanalysis *Electroanalysis* **17** 15–27

[40] Chang B Y and Park S M 2006 Integrated description of electrode/electrolyte interfaces based on equivalent circuits and its verification using impedance measurements *Anal. Chem.* **78** 1052–60

[41] Huang V M W, Vivier V, Orazem M E, Pébère N and Tribollet B 2007 The apparent constant-phase-element behavior of an ideally polarized blocking electrode *J. Electrochem. Soc.* **154** C81–8

[42] Jeng K T, Chien C C, Hsu N Y, Huang W M, Chiou S D and Lin S H 2007 Fabrication and impedance studies of DMFC anode incorporated with CNT-supported high-metal-content electrocatalyst *J. Power Sources* **164** 33–41

[43] Wang C H, Du H Y, Tsai Y T, Chen C P, Huang C J, Chen L C, Chen K H and Shih H C 2007 High performance of low electrocatalysts loading n CNT directly grown on carbon cloth for DMFC *J. Power Sources* **171** 55–62

[44] Reshetenko T V, Kim H T and Kweon H J 2008 Modification of cathode structure by introduction of CNT for air-breathing DMFC *Electrochim. Acta* **53** 3043–9

[45] Funakoshi T, Inoue T, Shimada H and Kojima S 1997 The mechanisms of nickel uptake by rat primary hepatocyte cultures: role of calcium channels *Toxicology* **124** 21–6

[46] Lobo A O, Antunes E F, Machado A H A, Pacheco-Soares C, Trava-Airoldi V J and Corat E J 2008 Cell viability and adhesion on as grown multi-wall carbon nanotube films *Mater. Sci. Eng.* C **28** 264–9

[47] Ryhänen J, Kallioinen M, Tuukkanen J, Junila J, Niemelä E, Sandvik P and Serlo W 1998 *In vivo* biocompatibility evaluation of nickel–titanium shape memory metal alloy: muscle and perineural tissue responses and encapsule membrane thickness *J. Biomed. Mater. Res.* **41** 481–8

[48] Bogdanski D, Köller M, Müller D, Muhr G, Bram M, Buchkremer H P, Stöver D, Choi J and Epple M 2002 Easy assessment of the biocompatibility of Ni–Ti alloys by *in vitro* cell culture experiments on a functionally graded Ni–NiTi–Ti material *Biomaterials* **23** 4549–55

[49] Van Harreveld A 1936 A physiological solution for freshwater crustaceans *Proc. Soc. Exp. Biol. Med.* **34** 428–32

[50] Krasne F B 1969 Excitation and habituation of the crayfish escape reflex: the depolarizing response in lateral giant fibres of the isolated abdomen *J. Exp. Biol.* **50** 29–46

[51] Yoon T H, Hwang E J, Shin D Y, Park S I, Oh S J, Jung S C, Shin H C and Kim S J 2000 A micromachined silicon depth probe for multichannel neural recording *IEEE Trans. Biomed. Eng.* **47** 1082–7